J. Fluid Mech. (1991), *vol.* 230, *pp.* 319–337
Printed in Great Britain

Phase decorrelation of coherent structures in a free shear layer

By CHIH-MING HO[1], YITSHAK ZOHAR[1], JUDITH K. FOSS[1] AND JEFFREY C. BUELL[2]†

[1] Department of Aerospace Engineering, University of Southern California, Los Angeles, CA 90089-1191, USA

[2] Center for Turbulence Research, NASA-Ames Research Center, Moffett Field, CA 94035, USA

(Received 10 November 1990 and in revised form 7 February 1991)

The vortices near the origin of an initially laminar mixing layer have a single frequency with a well-defined phase; i.e. there is little phase jitter. Further downstream, however, the phase jitter increases suddenly. Even when the flow is forced, this same transition is observed. The forcing partially loses its influence because of the decorrelation of the phase between the forcing signal and the passing coherent structures. In the present investigation, this phenomenon is documented and the physical mechanism responsible for the phase decorrelation is identified.

1. Introduction

The study of the mixing process of two fluids in a shear layer has been a major effort in turbulence research for decades. The concept of coherent structures proposed in the early 1970s (Crow & Champagne 1971; Brown & Roshko 1974; Winant & Browand 1974) changed the trend of the investigation. Since then, it has become clear that the evolution of the large vortical structures dominates the mass and momentum transfer across the two streams. These vortices have been identified as being quasi-periodic in the developed region of the mixing layer (Ho & Huerre 1984). In an unforced, laminar mixing layer or in a forced flow the initial vortices form in a periodic manner. The transition process from periodic to quasi-periodic flow was unknown and is studied here.

In the 1980s, several experiments showed that the entrainment of mass could be altered by manipulating the coherent structures. The spreading of the shear layer can be controlled either actively by applying periodic disturbances (Ho & Huang 1982; Oster & Wygnanski 1982; Lee & Reynolds 1985) or passively by modifying the initial geometry (Ho & Gutmark 1987). For cases where periodic perturbations are used to control the plane mixing layer, there exists a zone of influence, the extent of which depends on the velocity ratio and the hydrodynamic wavelength of the perturbation (Ho & Huerre 1984). Within this zone, the vortex merging pattern is phase locked to the control signal and the spreading rate is greatly changed. Beyond this region, however, the phase between the vortices and the forcing is no longer locked, and the forcing partially loses its influence. So, for improving control techniques, it is important to understand the physical mechanism of this phenomenon.

In this paper, an experimental study is presented to quantify the phenomenon of

† Present address: CENTRIC Engineering Systems, Inc., 3801 E. Bayshore Road, Palo Alto, CA 94303, USA.

phase jitter, to determine its downstream evolution as well as its dependence on the transverse and spanwise directions, and finally to identify the physical mechanism responsible for the phase decorrelation.

2. Apparatus and procedures

2.1. *Wind tunnel*

The experiments are conducted in an open-loop wind tunnel. Air is drawn through the tunnel by a blower providing suction downstream of the test section. A 3×3 m stilling chamber is separated into two independent sections by a 10 cm thick splitter plate. Four turbulence damping screens span the entire stilling chamber, while the splitter plate is constructed in sections and carefully sealed against each screen. The plate tapers uniformly through the contraction section at an angle of 2° on the low-speed side only. At the end of the contraction section, a steel plate is attached to the end of the splitter plate and terminates with an edge thickness of about 0.5 mm. The splitter plate divides the test section into two streams, each 30.5 cm deep and 91.4 cm wide. To obtain different velocity ratios between the upper and the lower streams, a series of cloth meshes placed over the upper half of the entrance to the stilling chamber produces an additional pressure drop and consequently a velocity difference at the plate trailing edge. A probe drive mechanism is housed in a large Plexiglas compartment resting on the roof of the tunnel. Probes are mounted on a vertical positioning drive and are introduced through an opening in the tunnel roof into the low-speed stream.

2.2. *Acoustic excitation*

Acoustic waves are generated to force the mixing layer. A row of 17 speakers spans the tunnel ceiling directly above the trailing edge of the splitter plate. The speakers are housed in a Plexiglas box lined with foam to damp any acoustic reflections. Each speaker input is individually amplified, and connects in parallel to a common source. The driving signal is provided by an electronic device, which can generate a sine wave of a given frequency and its subharmonics. The flow may be perturbed by any combination of the fundamental and its first and second subharmonics, where each amplitude and phase shift can be controlled. The acoustic field generated by this array of speakers is uniform across the span to within 5 dB, as measured by a microphone at the trailing edge, while the average intensity level is about 80 dB.

2.3. *Instruments and signal processing*

A single hot wire is used to measure the mean and fluctuating longitudinal velocity. The wire is made of 10% rhodium platinum and is 0.0025 mm in diameter, while the wire length varied from 1 to 1.5 mm. The constant-temperature hot-wire anemometer has a flat frequency response up to 30 KHz. The wire output voltage is calibrated using a Pitot tube to measure the corresponding velocity. The analogue output is digitized by a PDP 11/23 micro-computer at a rate higher than 100 times the passage frequency of the local large-scale structures. The fast-Fourier-transform (FFT) technique is used to compute the frequency spectra of the streamwise velocity. A time history of about 2000 structures is recorded at each station, and the mean value is then subtracted from the signal. This enables the detection of positively sloped zero crossings of the fluctuating component of the streamwise velocity. Subsequently, the period of each passing large-scale eddy is computed, and the periods of the entire population are used to construct a histogram. One or two lognormal distributions are

fitted to the measured histogram, where both the mean value and the standard deviation are determined using a least-squares method.

3. Mean flow quantities

3.1. *Initial conditions*

All experiments are conducted with laminar boundary layers on both sides of the splitter-plate trailing edge. Evidence for the state of the boundary layers at separation is obtained from traverses across the flow at $x = 0.25$ mm downstream of the plate trailing edge. Figure 1(*a*) compares the Blasius profile with the mean velocity distributions on both sides of the plate for the highest speed used for each stream. Frequency spectra of the streamwise velocity fluctuations inside both boundary layers at the trailing edge, plotted in figure 1(*b*), show that initially there exists wide-band background noise with no preferred frequency. The free-stream flow is uniform across the span to within 0.35% of the maximum velocity in either stream. The free-stream turbulent intensity level in the vicinity of the trailing edge is approximately 0.3% of the free stream.

3.2. *Mean velocity profiles*

The growth of the mixing layer is determined from the streamwise mean velocity distributions. The profiles measured at the midspan of the test section ($z = 0$) for free-stream velocities of $U_1 = 3.85$ m/s and $U_2 = 21.65$ m/s are shown in figure 2, where the velocity ratio is $R \equiv (U_2 - U_1)/(U_2 + U_1) = 0.7$. Close to the trailing edge the velocity profiles exhibit a wake-like defect. This is a result of the boundary layers on both sides of the splitter plate, which contain vorticity of opposite sign. Zhang, Ho & Monkewitz (1985) investigated the effects of the splitter-plate wake on the stability characteristics of the shear layer. They found that the instability process is dominated by the vorticity on the high-speed side with no substantial influence from the wake. Indeed, a short distance from the trailing edge the velocity defect disappears, and the profiles become monotonically varying. Further downstream the velocity distributions relax to a self-similar profile.

The initial lengthscale is the vorticity thickness, $\delta_0 \approx 2$ mm, based on the velocity profile at the trailing edge, as proposed by Zhang *et al.* (1985). The initial Reynolds number, based on the mean speed $\bar{U} = \frac{1}{2}(U_1 + U_2) = 12.75$ m/s, is then $Re = \bar{U}\delta_0/\nu = 1700$. The measured initial instability frequency is $f_0 = 880$ Hz, so that the initial Strouhal number based on the vorticity thickness is $St_0 = f_0\delta_0/\bar{U} = 0.138$, close to the value of 0.136 predicted by Monkewitz & Huerre (1982) for $R = 0.7$.

3.3. *Spreading of the mixing layer*

The momentum thickness can be obtained from the velocity distributions as follows:

$$\theta = \int_{-\infty}^{\infty} \left(\frac{U_2 - U}{U_2 - U_1}\right)\left(\frac{U - U_1}{U_2 - U_1}\right) \mathrm{d}y, \tag{1}$$

but only for those streamwise stations where the mean velocity profiles vary monotonically. However, the vorticity thickness, defined as

$$\delta \equiv \frac{U_2 - U_1}{(\partial U/\partial y)_{\max}}, \tag{2}$$

can be obtained for all streamwise stations, and is approximately four times that of

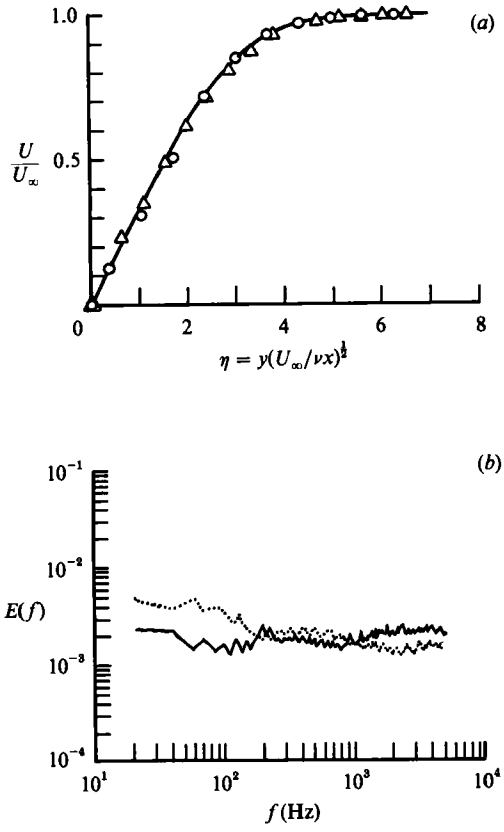

FIGURE 1. Boundary-layer characteristics at $z = 0$. (*a*) Velocity profiles: ○, $U_\infty = 24.25$ m/s (high-speed side); △, 9.15 m/s (low speed side). (*b*) Frequency spectra at $y = y(\frac{1}{2}U_\infty)$: ——, $U_\infty = 24.25$ m/s; ..., 9.15 m/s.

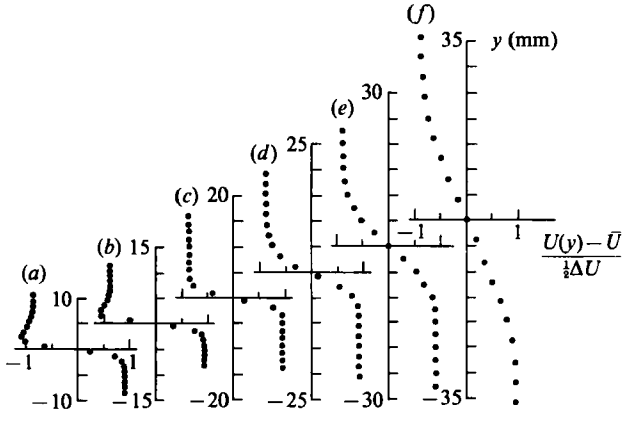

FIGURE 2. Mean velocity profiles for $R = 0.7$ at various X^*: (*a*) 0.56, (*b*) 1.1, (*c*) 2.2, (*d*) 4.5, (*e*) 6.7, (*f*) 13.4.

the momentum thickness for laminar flow. Thus, for stations close to the splitter-plate trailing edge, where a wake-like velocity defect still exists, the momentum thickness was estimated as $\theta \approx \frac{1}{4}\delta$. The results for two velocity ratios, $R = 0.7$ and 0.4, are shown in figure 3.

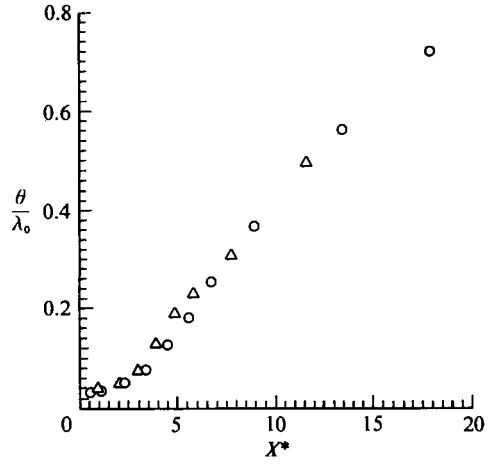

FIGURE 3. Downstream evolution of the momentum thickness for: △, $R = 0.4$; ○, $R = 0.7$.

The streamwise coordinate is normalized as $X^* = Rx/\lambda_0$, where λ_0 is the initial instability wavelength, $\lambda_0 = \bar{U}/f_0$. Based on this normalization, the first and second time-averaged vortex merging regions are at around $X^* = 4$ and 8, respectively (Ho & Huerre 1984; Huang & Ho 1990). The cross-stream coordinate is normalized by the local momentum thickness, $Y^* = y/\theta(x)$.

4. The phenomenon of phase decorrelation

4.1. *Passage of coherent structures in a natural mixing layer*

The convecting vortical structures induce potential velocity fluctuations outside the shear region. The hot wire positioned in this potential region senses the passage of the structures at a given streamwise location. Figure 4 shows hot-wire traces at six streamwise stations of a mixing layer with no artificial forcing. Here, the long-time average of the streamwise velocity, U, is subtracted from the total streamwise velocity component, u, to yield the fluctuating part, u'. The time records are four times the local average period, $\bar{T}(x)$, of the passing coherent structures, where the period T is the time interval between successive zero crossings with positive slopes. Close to the splitter-plate trailing edge, the signal is very well organized; i.e. the period of the passing coherent structures is nearly constant even in a natural shear layer. A short distance further downstream the periods start to fluctuate and become increasingly random.

Takaki & Kovasznay (1978) studied the probability distribution of large-scale vortex spacing in the fully turbulent region of the mixing layer. They derived a conservation equation for the distribution of spacings, in which the merging process results in the formation and destruction of these spacings. Their formulation included only amalgamations by pairing. The r.m.s. deviation of the probability distribution was found to be 0.39 times the average spacing. Following their lead, Bernal (1988) proposed a statistical theory of vortex circulation to describe the self-similar probability distribution from the vortex evolution properties. The model allows mergings not only by pairing, but also by tripling, etc. He suggested a lognormal distribution for the vortex spacings normalized by their streamwise location. His conclusion was that coalescence by pairing is the dominant form of

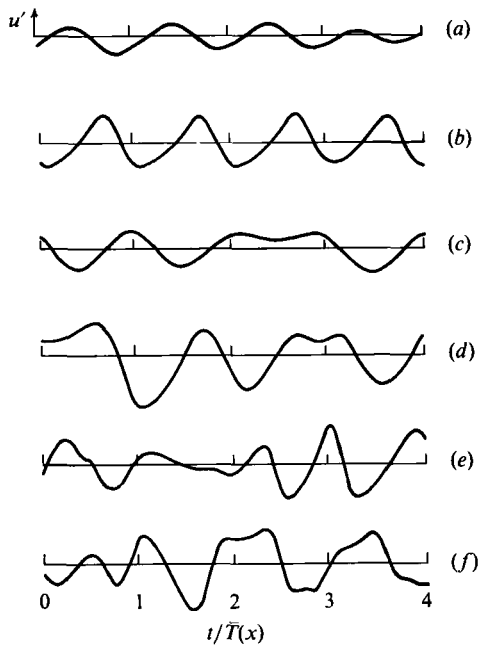

FIGURE 4. Traces of streamwise velocity fluctuations in time for $Y = 4$ and $R = 0.7$ at various X^*: (*a*) 1, (*b*) 2, (*c*) 4, (*d*) 6, (*e*) 8, (*f*) 16.

interaction, and the presence of other forms, such as tripling, increases the value of the standard deviation.

In this work, therefore, a lognormal distribution was also chosen to fit the data at all measured stations,

$$P(\tau) = \frac{1}{(2\pi)^{\frac{1}{2}}\sigma\tau}\exp\left[-\frac{1}{2}\left(\frac{\ln(\tau)-\mu}{\sigma}\right)^2\right], \tag{3}$$

where the standard deviation, σ, and the mean value of $\ln(\tau)$, μ, are calculated using the method of least squares to fit the experimental data. Here, the period of each coherent structure, T, is normalized by the local average period, $\bar{T}(x)$, to yield a non-dimensional period, τ, and $P(\tau)$ is the probability density function. The histograms are normalized so that the area below the curve is unity, since by definition $\int_{-\infty}^{+\infty} P(\tau)\,\mathrm{d}\tau \equiv 1$. When the data clearly show two peaks, the sum of two lognormal distributions is used and four parameters are calculated to fit the data. These histograms will be further explored for their dependence on the transverse, the spanwise and the streamwise directions.

4.2. *Dependence in the transverse direction*

The turbulent–non-turbulent boundary is a convoluted time-varying surface. If the hot wire is placed too close to the shear-layer centre, the zero-crossing histogram will be contaminated by the small eddies in the turbulent zone. If the probe is located too far into either free stream, the level of the induced velocity will be close to the background noise. Therefore, one has to examine the variation of the histograms in the transverse direction. The measured histograms along with the fitted distributions, at two downstream stations, $X^* = 1$ and 7, are shown in figure 5. Several cross-stream locations are plotted for each station. At the upstream station, $X^* = 1$, the histogram is very narrow with a sharp peak, whereas for the downstream station,

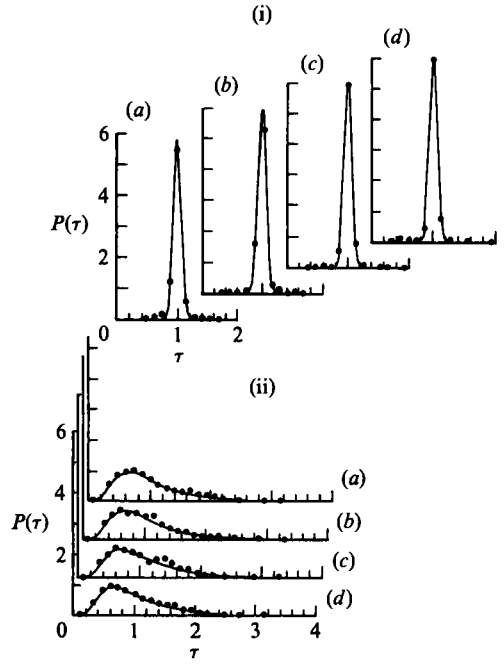

FIGURE 5. Coherent-structure histograms for $R = 0.4$ at various Y^*: (*a*) 4, (*b*) 6, (*c*) 8, (*d*) 10. (i) $X^* = 1$; (ii) $X^* = 7$. ●, Experiment; ——, lognormal fit (equation (3)).

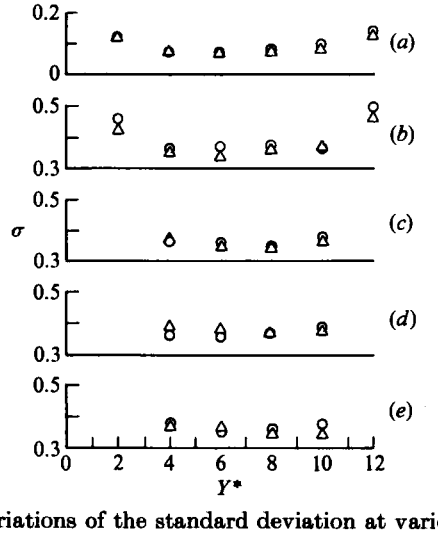

FIGURE 6. Transverse variations of the standard deviation at various X^*: (*a*) 2, (*b*) 4, (*c*) 6, (*d*) 8, (*e*) 12. ○, $R = 0.4$; △, $R = 0.7$.

$X^* = 7$, the distribution becomes broad and the peak is very shallow. Nevertheless, at both stations the distributions are nearly identical as the distance from the mixing-layer centre increases from $Y^* = 4$ to 10. The sharpness or broadness of these distributions can be represented by the magnitude of the standard deviation. The standard deviation is a quantitative measure characterizing the level of phase jitter at each station along the mixing layer. The standard deviation as a function of the transverse distance is plotted in figure 6 at five downstream locations for low and high velocity ratios, $R = 0.4$ and 0.7. At the two upstream stations, the standard

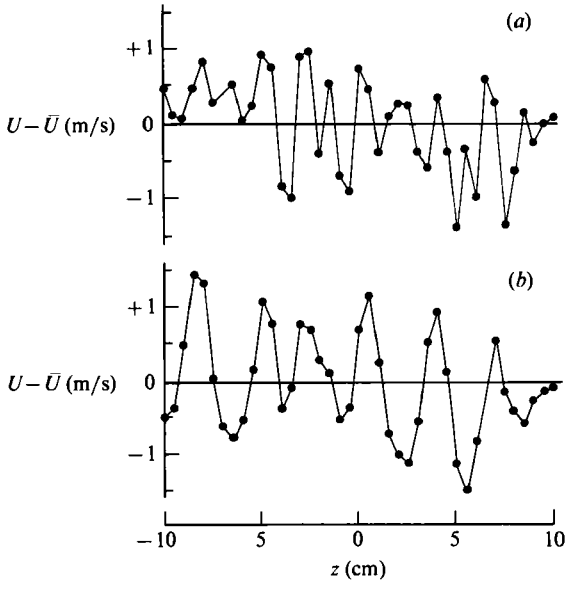

FIGURE 7. Spanwise velocity profiles for $R = 0.45$ and $Y^* = 5$ at: (a) $X^* = 5$, (b) $X^* = 8$.

deviation was obtained for wider range, $Y^* = 2$ to 12. Indeed, for small transverse locations, $Y^* < 4$, and large transverse locations, $Y^* > 10$, the phase jitter is larger since the zero crossing is affected by either the small turbulent eddies or the background noise. In the middle portion of the profile, the standard deviation is smaller and almost constant. This is because the recorded velocity signal in the intermediate region, in either the low- or high-speed side, corresponds primarily to the passing coherent structures. Consequently, their duration is independent of the cross-stream distance.

4.3. *Dependence in the spanwise direction*

The streamwise streaks in a mixing layer (Konrad 1976) are counter-rotating vortices (Bernal & Roshko 1986) which are stationary in the wind tunnel (Jimenez, Cogollos & Bernal 1985; Huang & Ho 1990). These localized vortices induce fluid from both the low- and the high-speed sides to cross the shear layer. Therefore, they result in a non-uniform spanwise distribution of the mean streamwise velocity, as shown in figure 7.

In order to check the dependence of the phase jitter in the spanwise direction, experiments were conducted with the probe located at several spanwise stations: at the cores of the vortices, the maximum and minimum velocity positions as well as points in between. The standard deviations of the phase jitter at $X^* = 2$ and 8 are shown in figure 8. The values are constant in the span for both the upstream and the downstream locations; thus the time-averaged phase-jitter levels are not influenced by the presence of the streamwise vortices.

4.4. *Dependence in the streamwise direction*

While the distribution of the normalized periods does not vary in the transverse and the spanwise directions, it does vary dramatically in the streamwise direction. Figure 9 shows the measured histograms with the fitted lognormal distributions at eight

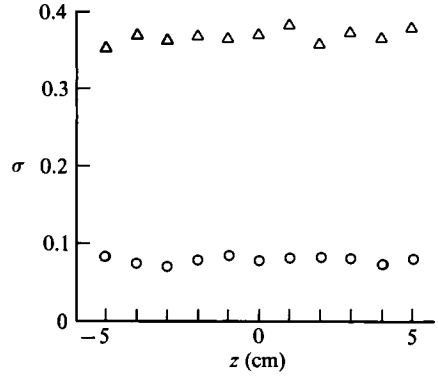

FIGURE 8. Spanwise variations of the standard deviation for $R = 0.45$ and $Y^* = 5$ at: ○, $X^* = 2$; △, $X^* = 8$.

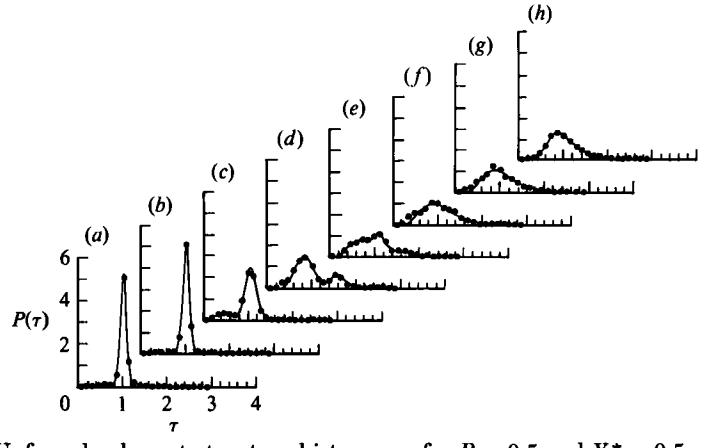

FIGURE 9. Unforced coherent-structure histograms for $R = 0.5$ and $Y^* = 0.5$ at various X^*: (*a*) 2, (*b*) 2.5, (*c*) 3, (*d*) 3.5, (*e*) 4, (*f*) 4.5, (*g*) 5, (*h*) 10. ●, Experiment; ——, lognormal fit (equation (3)).

streamwise stations for $R = 0.7$ and $Y^* = 5$. The distributions have a single peak and are very sharp in the initial region of the flow, $0.5 < X^* < 3$, where the roll-up and the formation process of the coherent structures take place (Ho & Huerre 1984). This indicates little phase jitter, since most of the periods have the same value. At $X^* = 3$, where the structures start to rotate around each other, the peak level of the histogram decreases sharply, and a second hump starts to develop at a period twice as long as the peak period. This type of histogram corresponds to the initial stage of the vortex merging process. Further downstream, at $X^* = 3.5$, the merging process is in progress resulting in a double-peaked distribution of almost the same probability, corresponding to the paired and unpaired structures. At $X^* = 4$, where the process is almost complete, the subharmonic mode takes over, leading to a shifted peak towards longer periods, though remnants of the fundamental mode still exist. At $X^* = 5$, the first vortex merging is complete and the distribution features a single peak once again, but its peak level is much lower in comparison with that in the initial region of the shear layer. Further downstream, $X^* > 5$, the histograms settle to a self-similar shape, where the most probable period increases continuously with the streamwise distance, reflecting the continuous decrease of the passage frequency as reported in previous investigations.

The larger width of the histogram at downstream stations indicates an increase in

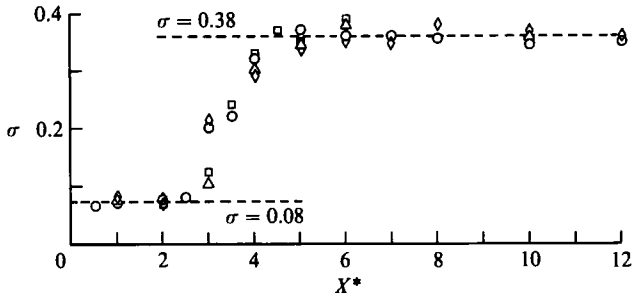

FIGURE 10. Downstream evolution of the standard deviation at $Y^* = 5$ for: ○, $R = 0.45$; □, $R = 0.5$; ◇, $R = 0.7$; △, $R = 0.8$.

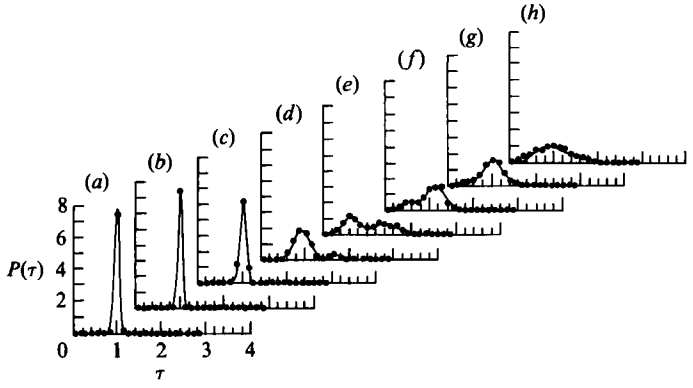

FIGURE 11. Forced coherent-structure histograms, f_0, for $R = 0.5$ and $Y^* = 5$ at various X^*: (*a*) 2, (*b*) 2.5, (*c*) 3, (*d*) 3.5, (*e*) 4, (*f*) 4.5, (*g*) 5, (*h*) 10. ●, Experiment; ——, lognormal fit (equation (3)).

the phase jitter of the coherent structures as is also shown in figure 4. The quantitative measure of this phase jitter, the standard deviation of the lognormal distribution, is plotted in figure 10 as a function of the downstream distance. The data points for a wide range of velocity ratios, $0.45 < R < 0.8$, all collapse onto one curve when the streamwise coordinate is normalized by R/λ_0 (Huang & Ho 1990). Close to the splitter plate, $X^* < 3$, the standard deviation is almost constant and small, about 0.08, corresponding to a low level of phase jitter. Then, in a short interval, $3 < X^* < 4$, the standard deviation more than quadruples. The abrupt increase in the phase jitter indicates that the phase information is lost downstream from this short region. This phenomenon is referred to as phase decorrelation. Once the phase information is lost, around the first vortex merging location, the standard deviation settles back to a constant value, about 0.38, which is much higher compared with the initial region. This suggests the existence of a self-similar region for the probability distributions, since the periods are normalized by the local mean period.

4.5. *Forcing effects*

The application of periodic excitation to a shear layer is commonly used to force the formation of the coherent structures at a more regular period than in a natural flow. In a forced case, a clearly defined phase reference is indeed obtained. Based on this phase reference, a phase-averaging technique can then be applied in various data analysis techniques. So now the phase decorrelation is examined in a forced flow.

Figure 11 shows the results for the case when the flow is forced at the fundamental frequency and all other parameters are identical to the naturally evolving case

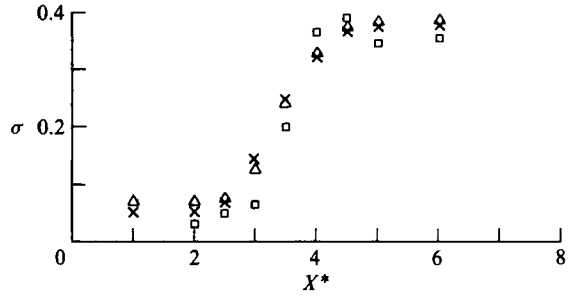

FIGURE 12. Standard-deviation evolution for $R = 0.5$: △, natural; □, forced at f_0; ×, numerical.

presented in figure 9. The histograms of the artificially forced mixing layer in the first stage, $X^* < 3$, are much sharper than those of the natural case. This is the result of the phase-locked large-scale structures which have a constant period. When the mixing layer is forced at the fundamental frequency (mode I in the experiment of Ho & Huang 1982), the vortex merging is delayed. This is evident from the location of the subharmonic hump. In the natural case (figure 9) it appears at $X^* = 3$, whereas in the forced case (figure 11) it appears further downstream at $X^* = 3.5$. Later on, the evolution of the phase jitter follows that of the natural case. As the first merging process takes place, the distribution becomes broader with a lower peak. Figure 12 shows the standard deviation as a function of the normalized downstream distance for the artificially excited and the natural mixing layer. Indeed, the standard deviation of the forced case in the initial region, about 0.05, is smaller than that of the natural case, about 0.08. Hence, applying forcing at the fundamental frequency of the mixing layer decreases the phase jitter significantly. Once the process of vortex merging is in progress, $3 < X^* < 4$, the standard deviations for the forced flow are in general lower than those for the natural case. However, their values increase greatly with the streamwise distance, so that the fundamental forcing is no longer effective in controlling the phase. Thus, phase decorrelation also occurs in a mixing layer forced at the fundamental frequency, and it occurs in the same streamwise region as for the natural flow. This finding suggests that even when a clear phase reference is artificially imposed upon the mixing layer, the phase information is still lost. For $X^* > 4$, the standard deviation reaches the same value as that in the unforced case, about 0.38, suggesting that there exists an asymptotic state for the phase jitter which is the same for forced and unforced case.

5. The origin of the phase decorrelation

There are several possible causes for this abrupt loss of the phase reference. Phase decorrelation could be a result of either a two- or a three-dimensional phenomenon. One possible scenario involves three-dimensional mechanisms such as the small-scale transition (Huang & Ho 1983) or the dislocation of spanwise structures (Browand & Troutt 1980). The fine eddies, which appear in the flow after the small-scale transition, can alter the vorticity distribution of the spanwise structures which in turn will modify the distance between vortex mergings (Pierrehumbert & Widnall 1982). In other words, the vortex-merging distance varies due to the random fine eddies and therefore can cause phase jitter of the coherent structures. The dislocation of vortices is a local deformation or pairing of vortices in the spanwise direction.

When a hot-wire probe measures the passing structures, the time trace will also show phase jitter. A second scenario is that the phase decorrelation may also be generated by two-dimensional mechanisms such as subharmonic instability or phase turbulence. The phase decorrelation is similar to the onset of phase turbulence encountered in a class of motions in which the loss of periodicity can be ascribed primarily to chaotic behaviour in the phase of the waves. The self-generated loss of phase reference, inherent in the dynamics of large-scale structures, will result in a broadband spectrum in the low-frequency range. Huerre (1987) proposed an amplitude evolution model to describe the development of instability waves in parallel free shear flows. His model shows that an array of spatially periodic coherent structures exhibits an Eckhaus-like instability dominated by two-dimensional disturbances. On the other hand, subharmonic instability appears when the subharmonic overtakes the fundamental as the most amplified mode (Kelly 1967), which results in the pairing of neighbouring coherent structures (Winant & Browand 1974). Monkewitz (1988) studied the spatial evolution of the fundamental mode and its subharmonic in a mixing layer. He found that after the initial exponential growth of the subharmonic, a resonant interaction between the two modes sets in the layer, resulting in a higher growth rate of the subharmonic. This nonlinear interaction leads to the excitation of a sideband of the subharmonic, i.e. of a pair of modes with a frequency ratio slightly deviating from 2:1. The first step in identifying the mechanism of phase decorrelation, therefore, is to determine whether it is primarily a two- or a three-dimensional phenomenon.

5.1. *A two-dimensional numerical simulation*

A numerical simulation of a two-dimensional, spatially evolving mixing layer forced at a single frequency was conducted by Ho *et al.* (1989) to investigate the phase decorrelation phenomenon. The two-dimensional incompressible Navier–Stokes equations are solved on a domain that is infinite in the cross-stream direction and finite in the streamwise direction. The pressure term is eliminated by taking the curl of the momentum equations twice and retaining only the x-component of the result. This yields a fourth-order equation for the streamwise velocity, u, which is advanced in time explicitly using a compact third-order Runge–Kutta scheme (Wray 1991). The vertical velocity, v, is recovered directly from the continuity equation.

The algorithm is based on a Fourier method with a cotangent mapping in the y-direction (so that the numerical domain $0 < \zeta < 1$ corresponds to the physical domain $-\infty < y < \infty$) and high-order-accurate Padé approximations in the x-direction. The first x-derivatives in the continuity equation and in the advection terms are approximated with modified Padé finite differencing (Lele 1991). The particular approximation used here yields sixth-order accuracy for low to moderate wavenumber components of the solution, and significantly smaller dispersion errors compared to standard differencing for high wavenumbers. The second- and fourth-order x-derivatives are approximated with classical fourth-order-accurate Padé formulae. The algorithm contains no numerical diffusion, which is believed to be important for problems where the dynamics is important and which contain many regions of strong gradients. Furthermore, without numerical diffusion, marginal resolution will usually appear as high-wavenumber oscillations and is thus easily detected. Details and numerical analytic tests of the scheme are presented in Buell (1991).

Like all spatially developing incompressible simulations, the present one must suffer from some degree of feedback between the outflow and inflow boundaries

(Buell & Huerre 1989). The convective outflow boundary condition (Buell 1991) passes large vortical structures fairly smoothly through the outflow boundary and thus minimizes the amplitude of the feedback. Forcing the inflow at a given frequency can thus easily overwhelm any feedback at that frequency. Given a sufficiently long computational domain, the remaining feedback is nearly indistinguishable from low-amplitude noise at the inflow boundary. Because of this noise, vortices can pair in a particular simulation even though the flow is forced with only the fundamental frequency and not the subharmonic. The feedback and noise are analogous to experimental wind tunnels where the change of tunnel geometry downstream of the test section can create feedback effects upstream, and the inflow to the test section always contains a certain level of free-stream turbulence.

For the present simulation, $Re = 100$, $R = 0.667$ and the length of the computational domain is $250\delta_0$. The Navier–Stokes equations are discretized using 385 uniformly spaced grid points in the streamwise direction and 168 Fourier modes in the mapped vertical coordinate. The low Reynolds number (an order of magnitude smaller than in the experiments) together with the fine grid ensure a well-resolved simulation. The mean inflow profile is based on the laminar self-similar solution and the forcing amplitude is $0.01(U_2-U_1)$.

The calculated velocity field is analysed in a manner similar to the experimental measurements. The phase jitter at each streamwise station is determined from the zero crossings of the velocity traces. The standard deviations of the phase jitter are plotted in figure 12. The level of phase jitter increases sharply around the first vortex merging location from less than 0.1 to about 0.4, close to the asymptotic value of 0.38 found in the experiments. In other words, the phase decorrelation can be reproduced not only qualitatively but also quantitatively by these calculations.

Since in these two-dimensional calculations the phase decorrelation still exists, one can conclude that it is a two-dimensional phenomenon. Three-dimensional effects, such as the small-scale transition (Huang & Ho 1990) or the vortex dislocation (Browand & Troutt 1980), will contribute to the phase jitter but cannot be its primary cause. The possible two-dimensional mechanisms modifying the phase of the large vortices are the Eckhaus and the subharmonic instabilities. The wavelength of the Eckhaus instability which can effectively influence the vortices is more than one order of magnitude longer than the initial wavelength of the coherent structures (Huerre 1987). However, the phase decorrelation occurs after three coherent-structure wavelengths from the origin of the mixing layer. Therefore, the Eckhaus instability cannot generate the phase jitter observed here. Subharmonic instability governing the vortex merging then becomes the most probable candidate.

5.2. *Phase decorrelation and subharmonic instability*

The phase decorrelation occurs between $X^* = 2.4$ and 4, which is the region from the onset to the end of the first vortex merging (Huang & Ho 1990). The effect of vortex merging on the phase jitter is examined by band-pass filtering a time history of streamwise velocity fluctuations of a mixing layer forced at the fundamental frequency. The velocity trace is recorded at $X^* = 3.5$, where the vortex merging and hence the phase decorrelation is in progress. The raw signals shown in figure 13(*a*) come from both the experimental and numerical data, and at this station are a combination of the fundamental and the subharmonic modes. The raw signal passed either a filter with a band centred around the fundamental frequency (figure 13*b*), or a filter with a band centred around the first subharmonic frequency (figure 13*c*). Their frequency spectra are shown in figure 14 (*a–c*), respectively. The total signal at

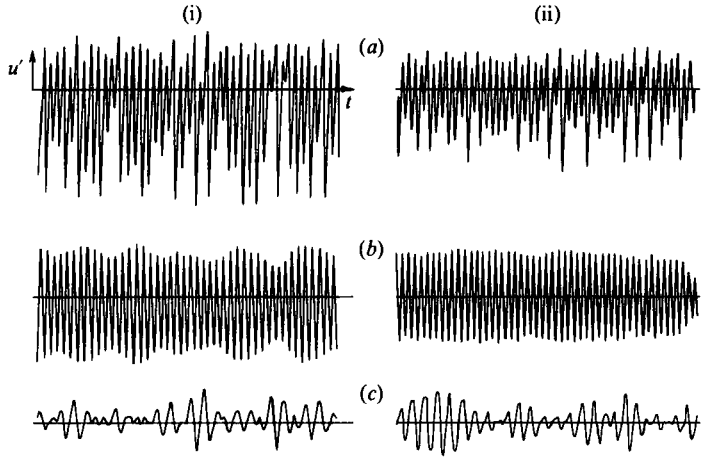

FIGURE 13. Time traces of streamwise velocity fluctuations at $X^* = 3.5$. (i) Experiment; (ii) numerical simulation. (*a*) Raw signal, (*b*) filtered around f_0, (*c*) filtered around $\frac{1}{2}f_0$.

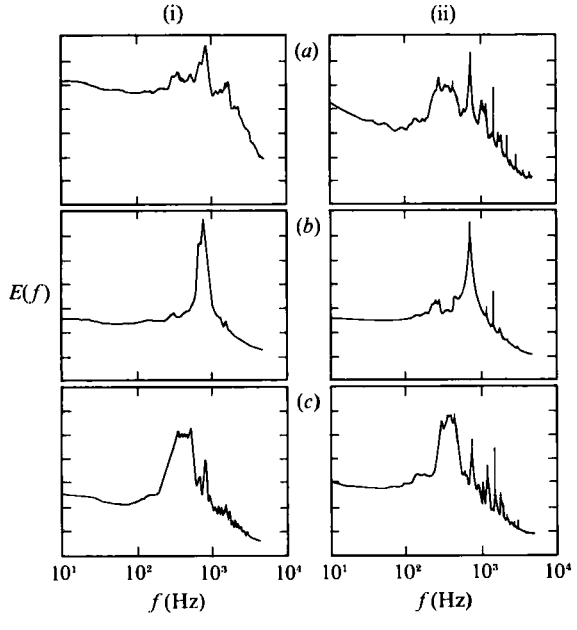

FIGURE 14. Energy spectra corresponding to figure 13.

this location (figure 13*a*) is not as regular as those at $X^* = 1$ and 2 (figure 4). On the other hand, the fundamental (figure 13*b*) has an almost constant amplitude and the spectral peak is sharp, in contrast with the subharmonic peak which has a wide band (figure 14*c*). It is then clear that the large phase jitter is primarily due to the subharmonic mode (figures 13*c* and 14*c*).

The initial growth of the subharmonic modes is a linear process (Ho & Huerre 1984). As the shear layer becomes thicker with streamwise distance, the amplification rate of the subharmonics also increases. A wide band of perturbations around the subharmonics is amplified from the background noise as well. Therefore, the

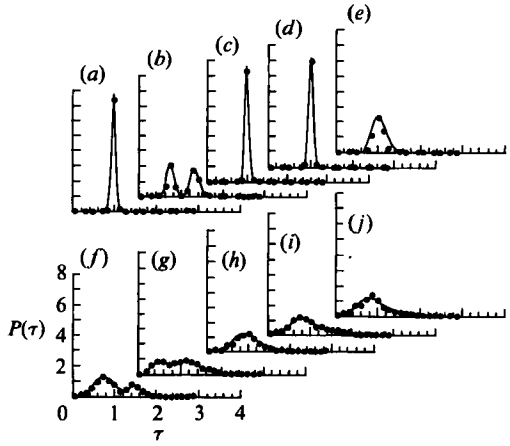

FIGURE 15. Forced coherent-structure histograms, $f_0+\frac{1}{2}f_0$, for $R = 0.6$ and $Y^* = 5$ at various X^*: (*a*) 2, (*b*) 3, (*c*) 4, (*d*) 5, (*e*) 6, (*f*) 7, (*g*) 8, (*h*) 9, (*i*) 10, (*j*) 20. ●. Experiment; ——, lognormal fit (equation (3)).

subharmonic modes do not have an exact phase relationship with the fundamental. These phase differences result in amplification rate variations (Zhang *et al.* 1985) and in different vortex evolution patterns, pairing or shredding. Consequently, the phase jitter increases. The rest of the amplified modes, other than the subharmonic, lead to variations of the vortex merging location as a function of the frequency, which add to the phase jitter.

Downstream of the linear growth region the subharmonic mode receives energy from the fundamental via the subharmonic resonance mechanism (Kelly 1967; Monkewitz 1988). Monkewitz (1988) suggested a detuning phenomenon of the subharmonic waves in his weakly nonlinear analysis. The detuning produces two sidebands which can be seen in both the experimental and the numerical spectra (figure 14*c*). The difference between the sideband frequencies and the subharmonic is $\pm 0.11 f_0$ in the present mixing layer, $R = 0.7$, which is close to the predicted value of 0.08 for $R = 1$ flows. In summary, the nonlinear effect of the sidebands along with the linear effect of the wide-band growth lead to the phase decorrelation. Therefore, one cannot inhibit phase decorrelation just by pure monochromatic forcing.

5.3. *Extent of zone of influence*

When the mixing layer is forced at its fundamental frequency, the zone of influence ends around the first vortex merging, because the naturally generated subharmonic waves are not exactly phase locked with the forcing signal. This point can be further illustrated by forcing the flow at the fundamental and the first subharmonic frequencies with a definite phase reference. In this case, the zone of influence indeed increases, and the phase decorrelation occurs further downstream. Zhang *et al.* (1985) studied the response of a mixing layer forced by both the fundamental and the subharmonic at various phase differences, β. They reported that the amplification rate of the subharmonic is maximum when the two frequencies are in phase, $\beta = 0$, and minimum when out of phase, $\beta = \pi$. For this reason, the fundamental and the subharmonic forcing frequencies in the present experiment have the same amplitude and zero phase shift. The histograms of the phase jitter are plotted in figure 15. Initially, the phase jitter is very small. Around $X^* = 3$, the first vortex merging

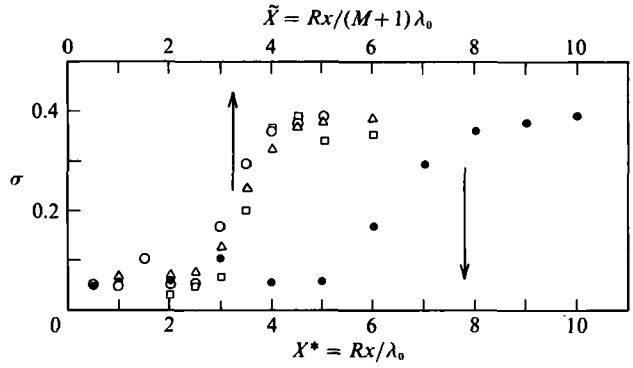

FIGURE 16. Streamwise evolution of the standard deviation at $Y^* = 5$: △, natural; □, forced, f_0; ●, forced, $f_0+\frac{1}{2}f_0$(σ *vs.* X^*); ○, forced, $f_0+\frac{1}{2}f_0$(σ *vs.* $\tilde{X}$).

occurs and is indicated by the double peak in the histogram. The most interesting histograms are those downstream of the first vortex merging but upstream of the second vortex merging, $X^* = 4$ and 5, where they have a single sharp peak indicating little phase jitter. Here the phase decorrelation is detected around the second vortex merging location. The corresponding standard deviations are shown in figure 16. The high-level phase-locked subharmonic imposed by the forcing suppresses the phase jitter caused by both the linear and nonlinear effects. Therefore, the phase decorrelation is delayed to the amplification region of the second subharmonic, and the zone of influence is doubled compared with that of the flow forced at the fundamental only. If the wavelength of the forced subharmonic is used as the normalizing lengthscale, $\tilde{X} = Rx/2\lambda_0$, the three curves corresponding to the natural flow, the flow forced at fundamental only and the flow forced at fundamental and first subharmonic, collapse onto a single curve. It seems that if the flow is forced at the Mth subharmonic, the zone of influence can be increased to the region of $(M+1)$th vortex merging. However, the three-dimensional feature of the spanwise structures, e.g. the influences of dislocation and small-scale eddies, becomes strong after the second vortex merging region. Therefore, when the flow is forced at a low amplitude, it becomes increasingly difficult to extend indefinitely the zone of influence by perturbing the mixing layer at increasingly lower subharmonics.

5.4. *Stages of transition*

A laminar mixing layer originates with periodic instability waves and eventually reaches a fully turbulent state. The flow undergoes many stages of transitions which are summarized in figure 17 (Ho *et al.* 1988). The Kelvin–Helmholtz instability waves gain energy from the free stream and roll up into a spanwise vortex at $X^* = 2$. Simultaneously, low-frequency perturbations also grow in this region but with a smaller growth rate. Just downstream, the growth rate of the subharmonic increases via energy transfer from the fundamental. However, the presence of the other unstable modes leads to phase jitter between the fundamental and the subharmonic mode. Therefore, if the phase between these two modes is not forced, the first vortex merging is not phase locked. Consequently, the phase of the merged vortices becomes random due to the phase decorrelation around $X^* = 3$. The process of vortex merging, around $X^* = 4$, involves intense interaction between the streamwise and the spanwise vortices, which triggers the production of small-scale eddies (Huang & Ho 1983). Thus, the small-scale transition takes place between $4 < X^* < 8$,

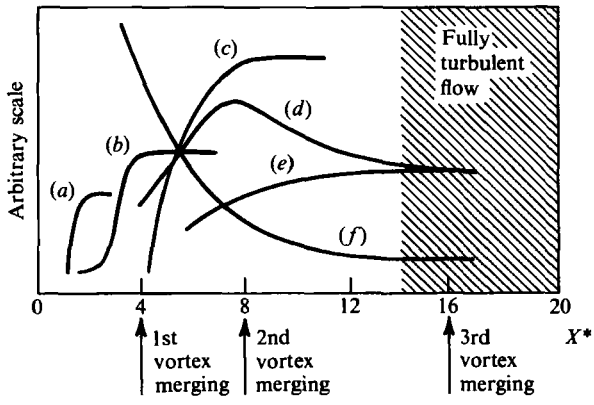

FIGURE 17. Sequence of transitions in a mixing layer: (*a*) growth of low-frequency perturbation (Ho *et al.* 1988); (*b*) phase decorrelation (present study); (*c*) small-scale transition (Huang & Ho 1983); (*d*) turbulence level of initially laminar boundary layer (Bradshaw 1966); (*e*) turbulence level of initially turbulent boundary layer (Bradshaw 1966); (*f*) spanwise separation for 40% correlation (Browand & Troutt 1980).

downstream of the phase decorrelation region. This provides further support that the sudden increase of the phase jitter is not the result of the three-dimensional random eddies.

The initial boundary-layer conditions, laminar or turbulent, have long-lasting influences on the development of the mixing layer. Although the inertial subrange is well established by the second vortex merging, $X^* > 8$, the flow has not yet reached the fully developed turbulent state. For flows originating with either laminar or turbulent conditions, both the spreading rate and the peak turbulence intensity approach an asymptotic state near the third vortex merging at $X^* = 16$ (Bradshaw 1966). Browand & Troutt (1980) measured the spatial spanwise correlation to characterize the two-dimensionality of the spanwise structure. Indeed, they found that the correlation coefficient decreases with streamwise distance and reaches an asymptotic value at around $X^* = 15$. Downstream of this region, after the mixing layer has undergone all the transitions, the layer reaches the equilibrium state of fully developed turbulent flow.

6. Conclusions

In this study, it was found that even though the passage of the coherent structures originally has a well-defined frequency, the phase suddenly becomes random around the first vortex merging region. The phase decorrelation ends the zone of influence of the artificial forcing. This zone of influence, however, can be extended by forcing the subharmonics as well as the fundamental frequencies. The mechanism responsible for the phase decorrelation is the loss of the exact phase reference between the fundamental and the subharmonic modes during the growth of the subharmonics.

This work is supported by a contract from the Office of Naval Research.

REFERENCES

Bernal, L. P. 1988 The statistics of the organized structures in turbulent mixing layer. *Phys. Fluids* **31**, 2533–2543.

Bernal, L. P. & Roshko, A. 1986 Streamwise vortex structure in plane mixing layers. *J. Fluid Mech.* **170**, 499–525.

Bradshaw, P. 1966 The effects of initial conditions on the development of a free shear layer. *J. Fluid Mech.* **109**, 1–24.

Browand, F. K. & Troutt, T. R. 1980 A note on spanwise structure in the two-dimensional mixing layer. *J. Fluid Mech.* **97**, 771–781.

Brown, G. L. & Roshko, A. 1974 On density effects and large structure in turbulent mixing layer. *J. Fluid Mech.* **64**, 775–816.

Buell, J. C. 1991 A hybrid numerical method for three-dimensional spatially-developing free-shear flows. *J. Comp. Phys.* (to appear).

Buell, J. C. & Huerre, P. 1989 Inflow/outflow boundary conditions and global dynamics of spatial mixing layers. In *Studying Turbulence Using Numerical Simulation Databases-II, Proc. 1988 Summer Program of the Center for Turbulence Research, Rep.* CTR-S88, pp. 19–27.

Crow, S. C. & Champagne, F. H. 1971 Orderly structure in jet turbulence. *J. Fluid Mech.* **48**, 545–591.

Ho, C. M. & Gutmark, E. 1987 Vortex induction and mass entrainment in a small-aspect-ratio elliptic jet. *J. Fluid Mech.* **179**, 383–405.

Ho, C. M. & Huang, L. S. 1982 Subharmonics and vortex merging in mixing layers. *J. Fluid Mech.* **119**, 443–473.

Ho, C. M. & Huerre, P. 1984 Perturbed free shear layers. *Ann. Rev. Fluid Mech.* **16**, 365–424.

Ho, C. M., Zohar, Y., Foss, J. K. & Huang, L. S. 1988 Transition processes of mixing layers. *Proc. 2nd European Turbulence Conference.* Springer.

Ho, C. M., Zohar, Y., Moser, R. D., Rogers, M. M., Lele, S. K. & Buell, J. C. 1989 Phase decorrelation, streamwise vortices and acoustic radiation of mixing layers. In *Studying Turbulence Using Numerical Simulation Databases-II, Proc. 1988 Summer Program of the Center for Turbulence Research, Rep.* CTR-S88, pp. 29–39.

Huang, L. S. & Ho, C. M. 1983 Development of free shear layer. In *IUTAM Symp. on Turbulence and Chaotic Phenomena in Fluids, Kyoto, Japan* (ed. T. Tatsumi), pp. 327–332. North-Holland.

Huang, L. S. & Ho, C. M. 1990 Small scale transition in a plane mixing layer. *J. Fluid Mech.* **210**, 475–500.

Huerre, P. 1987 Evolution of coherent structures in shear flows: a phase dynamic approach. *Nuclear Phys.* B (Proc. Suppl.) **2**, 159–178.

Jimenez, J., Cogollos, M. & Bernal, L. P. 1985 A perspective view of the plane mixing layer. *J. Fluid Mech.* **152**, 125–143.

Kelly, R. E. 1967 On the stability of an inviscid shear layer which is periodic in space and time. *J. Fluid Mech.* **27**, 657–689.

Konrad, J. H. 1976 An experimental investigation of mixing in two-dimensional turbulent shear flows with applications to diffusion-limited chemical reactions. *Tech. Rep. Inter. Rep.* CIT-8-PU. California Institute of Technology.

Lee, M. & Reynolds, W. C. 1985 Bifurcating and blooming jet. *Tech. Rep. TF*-22. Stanford University.

Lele, S. K. 1991 Compact finite difference schemes with spectral-like resolution. *J. Comp. Phys.* (submitted).

Monkewitz, P. A. 1988 Subharmonic resonance, pairing and shredding in the mixing layer. *J. Fluid Mech.* **188**, 223–252.

Monkewitz, P. A. & Huerre, P. 1982 The influence of the velocity ratio on the spatial instability of mixing layers. *Phys. Fluids* **25**, 1137–1143.

Oster, D. & Wygnanski, I. 1982 The forced mixing layer between parallel streams. *J. Fluid Mech.* **123**, 91–130.

Pierrehumbert, R. T. & Widnall, S. E. 1982 The two- and three-dimensional instabilities of a spatially periodic shear layer. *J. Fluid Mech.* **114**, 59–82.

TAKAKI, R. & KOVASZNAY, L. S. G. 1978 Statistical theory of vortex merger in the two-dimensional mixing layer. *Phys. Fluids* **21**, 153–156.

WINANT, C. D. & BROWAND, F. K. 1974 Vortex pairing: the mechanism of turbulent mixing layer growth at moderate Reynolds number. *J. Fluid Mech.* **63**, 237–255.

WRAY, A. A. 1991 Minimal storage time-advancements schemes for spectral methods, *J. Comp. Phys.* (submitted).

ZHANG, Y. Q., HO, C. M. & MONKEWITZ, P. A. 1985 The mixing layer forced by fundamental and subharmonic. In *IUTAM Symp. on Laminar-Turbulent Transition, Novosibirsk* (ed. V. Kozlov), pp. 385–395. Springer.